

Formation and structure of 360 and 540 degree domain walls in thin magnetic stripes

Youngman Jang,^{1,a)} S. R. Bowden,² Mark Mascaro,¹ J. Unguris,² and C. A. Ross^{1,b)}

¹Department of Materials Science and Engineering, Massachusetts Institute of Technology, Cambridge, Massachusetts 02139, USA

²Center for Nanoscale Science and Technology, National Institute of Standards and Technology, Gaithersburg, Maryland 20899, USA

(Received 23 November 2011; accepted 15 January 2012; published online 10 February 2012)

360°, 540°, and other complex transverse domain walls have been created in narrow cobalt wires connected to injection pads by cycling a magnetic field perpendicular to the wire length. The composite walls, formed by impingement of 180° transverse walls of alternating chirality, are stable over a wide field range. The structure of the walls observed at remanence by scanning electron microscopy with polarization analysis and by magnetic force microscopy is in good quantitative agreement with the prediction of micromagnetic simulations. © 2012 American Institute of Physics. [doi:10.1063/1.3681800]

360° domain walls (360DWs) represent a special class of walls separating magnetic domains that have parallel magnetization directions. The formation of a 360DW does not significantly reduce the stray field of a magnetized material, and the 360DW itself has a wall energy. 360DWs, therefore, increase the total energy of a magnetic system and, as a result, may be expected to be rare. However, 360DWs have been commonly observed in a range of thin film magnetic materials.¹⁻⁴ They are metastable and can be present over a wide range of fields, including at remanence. In a continuous thin film, 360DWs can be formed when Bloch lines present in 180° Néel walls are pinned at defects. An applied field then causes the impingement of two 180° Néel wall segments with the same sense of rotation ('winding walls').²⁻⁵ Once formed, 360DWs require a high field to annihilate them, and they have profound effects on the subsequent reversal behavior of the film.

The formation of 360DWs in patterned magnetic films and multilayers has been investigated more recently.⁶⁻¹² Patterned films are important in a range of magnetic devices, including magnetic random access memories¹³ and domain wall devices such as DW logic¹⁴ or racetrack memory¹⁵ in which 180° walls (180DWs) representing bits of data are moved around a magnetic circuit, and rotation sensors¹⁶ where a rotating magnetic field injects 180DWs into a wire. In patterned structures, 360DWs often form by the combination of two winding 180° Néel walls, for example, when one 180° wall moves around a thin film ring and meets another 180° wall¹⁷ or when 180° walls are successively injected into a wire by a rotating field.¹⁸ As in the case of continuous films, the presence of 360DWs in patterned films dramatically affects the switching behavior, but in addition, the stray fields produced by the 360DWs can affect the behavior of adjacent magnetic layers.⁹ This magnetostatic interaction could be used to provide a programmable pinning site for wall motion in an adjacent layer, for example. Additionally,

modeling shows that the current-induced domain wall motion of a 360DW differs qualitatively from that of its constituent 180DWs,¹⁹ and therefore the combination of 180DWs into 360DWs will have a major effect on the operation of devices based on current-driven domain wall motion.

It is, therefore, important to understand the formation, the structure, and the stray field distribution of 360DWs in narrow magnetic thin film stripes. In this article, the formation of 360DWs, 540° walls (540DWs) and other complex domain wall structures is demonstrated by injection of 180DWs from a circular pad into a narrow wire using an alternating in-plane field. The magnetization orientation within the wall is investigated using scanning electron microscopy with polarization analysis (SEMPA), the magnetic field distribution is imaged using magnetic force microscopy (MFM), and the structure and stray fields are compared with micromagnetic simulations.

The structure consisted of a circular pad attached asymmetrically to a gently curved wire, in contrast to the symmetrical structure used by Diegel *et al.*¹⁶ The asymmetrical placement determined the chirality of 180DWs formed by field cycling. The circular pad was 1.2 μm in diameter and the wire was 250 nm wide, patterned on a Si substrate from a magnetron sputtered film of Ti(5 nm)/Co(6 nm)/Au(5 nm) by electron beam lithography and lift-off.

The magnetic states of the nanostructures were imaged at remanence by magnetic force microscopy (MFM) using a low-moment commercial tip scanned at 20 nm to 100 nm lift height. In-plane fields were applied prior to imaging. SEMPA (Refs. 20 and 21) was used to image the 3-dimensional spin orientation of the samples. For transition metal ferromagnets such as Co, where electron spin dominates the contribution to magnetization, the secondary electron polarization is directly proportional to the magnetization, and SEMPA produces an image of the magnetic nanostructure. The probing depth of SEMPA is 1 nm; so, SEMPA measurements were made in ultrahigh vacuum (UHV) with a base pressure less than 3×10^{-8} Pa after cleaning the samples by sputtering *in situ* with 800 eV to 1000 eV Ar ions while monitoring the surface composition with Auger spectroscopy. Sputtering removed

^{a)}Present address: Samsung Advanced Institute of Technology (SAIT), Gyeonggi-Do 446-712, South Korea.

^{b)}Electronic mail: caross@mit.edu.

any oxide or hydrocarbon contamination, as well as the Au capping layer. After cleaning, a 0.5 nm thick Fe layer was deposited on the sample to increase the polarization contrast and decrease charging from the surrounding SiO₂. All SEMPA images were measured at remanence. To apply magnetic fields, the sample was transferred to an adjoining UHV chamber, which contained an electromagnet. The SEMPA instrument uses two orthogonal low-energy diffuse-scattering Mott polarization analyzers to measure all three components of the polarization vector.²⁰

To verify the formation of 360DWs in the structure, micromagnetic simulations using the OOMMF micromagnetics package²² were performed for a Co nanostructure which consisted of a circular pad of 1.2 μm diameter connected to a curved wire of 120 nm width, 2 μm length, and 5 nm thickness. The model used rectangular unit cells of no larger than 4 nm × 4 nm × 5 nm and standard material parameters of Co: 1.4 × 10⁶ A/m for saturation magnetization, 0.01 for the damping constant, and 3.0 × 10⁻¹¹ J/m for exchange stiffness. After saturation with an in plane *y*-direction magnetic field (*H_y*) of 239 kA/m, a head-to-head transverse²³ 180DW was formed in the wire at remanence, shown in Fig. 1(a). To inject a second transverse 180DW, *H_y* was increased from 0 kA/m to -9.5 kA/m in 24 steps of 1 ns duration. Injection of the second 180DW occurred at *H_y* = -4.0 kA/m (Fig. 1(b)) and the two 180DWs combined into a 360 DW (Fig. 1(c)), but the field was then increased to -9.5 kA/m in order to eliminate the vortex from the injection pad, which was necessary before additional 180DWs could be injected on subsequent cycles. The 360DW was stable at 9.5 kA/m. This process could therefore be used to stack several 180DWs into the wire by alternating *H_y* between ±9.5 kA/m (Fig. 1(d)).

To demonstrate the formation of 360DWs in an experimental system, a Co sample was saturated at *H_y* = 239 kA/m, returned to remanence to form a 180DW, and then

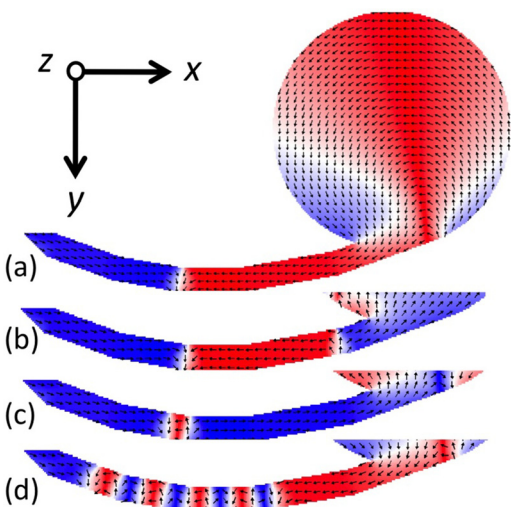


FIG. 1. (Color online) OOMMF model of formation of 360DW in a wire attached to a circular pad. (a) After 239 kA/m saturation along *y*, a 180DW formed in the wire, shown at remanence. (b) A further field of -4.0 kA/m along *y* produced a second 180DW. (c) The remanent state showing a 360DW. (d) Repeated alternating field of magnitude 9.5 kA/m along *y* generated multiple domain walls. Red and blue (or greyscale shading) represent the sign of the *x*-component of the magnetization.

H_y = -15.9 kA/m was applied to inject a second 180DW. Fig. 2(a) shows an MFM image at 20 nm tip height of the remanent 360DW, indicated by the dark-light contrast. A SEMPA image of the same sample is shown in Fig. 2(b). This is a direct image of the surface magnetization of the sample, which displays a continuous rotation of the magnetization angle on traversing the wall. Fig. 2(c) plots the angle of the magnetization as a function of distance across the wire, showing that the DW has ‘tails’ extending along the wire similar to the tails of a 180DW. The equilibrium width of the 360DW (estimated as the distance within which the magnetization angle changes by 80% of 360°, i.e., from -144° to +144°) was ≈ 350 nm. This width is determined by a balance between the magnetostatic interaction between the two component 180DWs, which pulls the 180DWs together, and the exchange energy at the center of the 360DW, which pushes them apart.

The origin of the MFM contrast can be understood by modeling the stray field of the 360DW. A micromagnetic

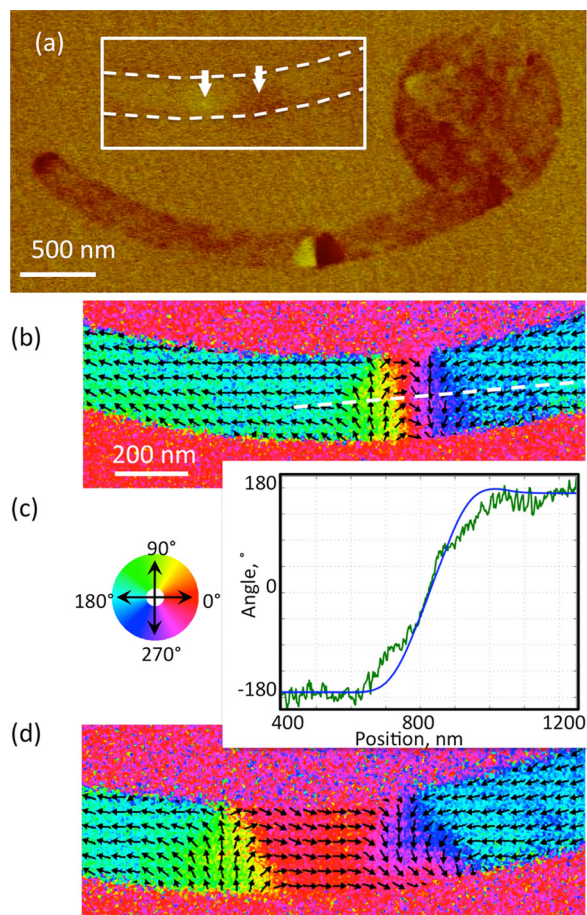


FIG. 2. (Color online) (a) MFM data of a 360DW imaged at a tip height of 20 nm. The 360DW shows as two contiguous bright and dark contrast regions, and the shapes of the wire and injection pad are evident. The inset shows part of another sample imaged at a height of 100 nm in which two spatially separated 180DWs are present, indicated by arrows, one with bright contrast and one with dark contrast, but they do not form a 360DW. The contrast is weaker but a larger separation between the dark and light contrast is evident. (b) SEMPA image of the sample of (a) with the in-plane magnetization direction indicated on a color wheel. (c) The angle between the magnetization and the axis of the wire, measured along the dashed line shown in (b) (green, noisy curve) and calculated from the micromagnetic simulation of Fig. 3(a) (blue, smooth curve). (d) SEMPA image of the sample in the inset of (a), showing a pair of separated 180DWs. The uncertainty in the magnetization direction for the SEMPA data is 17.1° (one standard deviation).

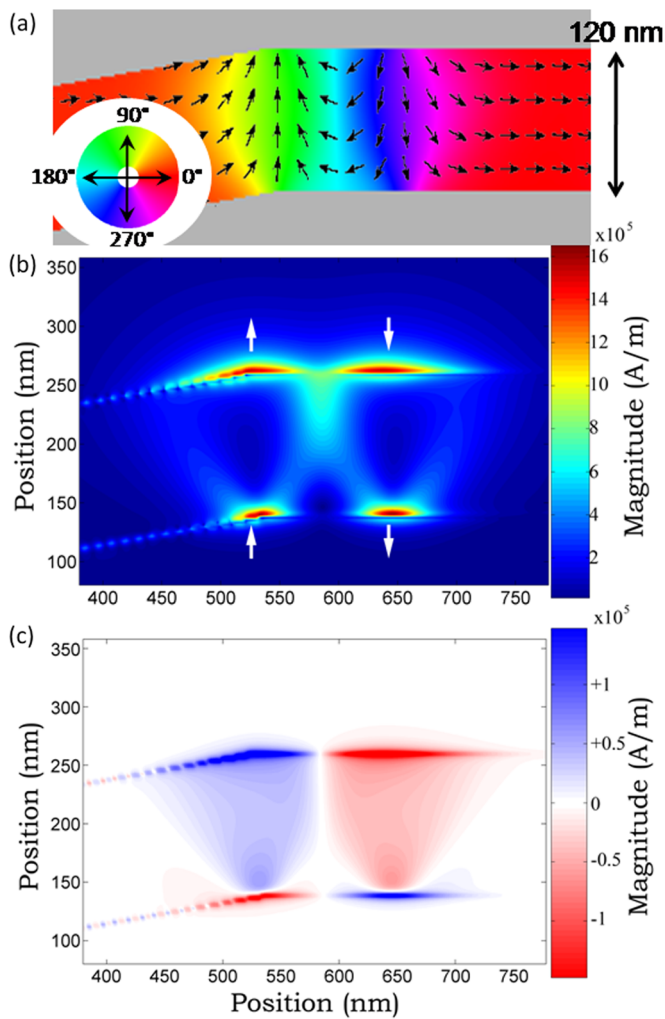


FIG. 3. (Color online) (a) oommf simulation of a 360DW in a wire. The magnetization directions are plotted on a color wheel. (b) In-plane stray field magnitude calculated at a height of 3 nm above the surface of the sample. The white arrows represent the in-plane direction of the field at its greatest magnitude. (c) Calculated z -component of the stray field at a height of 3 nm above the surface of the sample.

simulation of the 360DW is shown in Fig. 3(a) based on a wire shape modeled using a mask created from two rectangles joined with a 20° angle to approximate the curve in the wire, digitized into $2 \text{ nm} \times 2 \text{ nm} \times 6 \text{ nm}$ thick Co cells. Fig. 3(b) shows the in-plane magnitude $(H_x^2 + H_y^2)^{0.5}$ of the stray field of the 360DW calculated at a height of 3 nm above the surface of the Co film, and Fig. 3(c) shows the out-of-plane component H_z . The 360DW produced a field similar to that of a superposed dipole and quadrupole. The stray field was substantial in the vicinity of the wire but decayed rapidly away from the wire. The MFM contrast is sensitive to the H_z component at the scan height and produced a dark-light contrast, which is asymmetrical with respect to the axis of the wire.²⁴ The magnetization angle vs distance along the wire is shown in Fig. 2(c) and agrees well with the experimental data.

In contrast to the 360DW of Fig 2(b), whose structure agrees well with that of the micromagnetic simulation in Fig. 3(a), we also observed a wider structure shown in Fig. 2(d) in a different sample. The MFM image of this sample, measured at a scan height of 100 nm, is shown as the inset of Fig. 2(a). The two component 180DWs are separated from each other, presumably as a result of pinning in the wire, and this

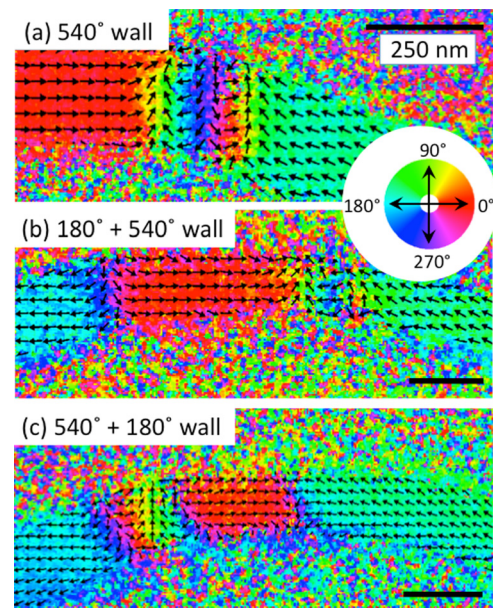


FIG. 4. (Color online) (a) SEMPA image of a 540DW. (b) SEMPA image after injecting an additional 180DW. (c) A 540DW of opposite sense to that of (a) adjacent to a 180DW. Magnetization directions are indicated on a color wheel. The uncertainty in the SEMPA angular data is 7.4° (one standard deviation). Scale bars are 250 nm.

structure does not represent an equilibrium 360DW. Unlike the equilibrium 360DW, the structure of Fig. 2(d) was destroyed during MFM scanning at a tip height of 90 nm, presumably because the tip field displaced the 180DWs and facilitated their recombination.

The injection pad/wire structure could also be used to demonstrate the formation and stability of more complex DWs, as predicted in Fig. 1(d). A 540DW was formed by applying field steps in the SEMPA vacuum chamber before imaging. $H_y = 134 \text{ kA/m}$ was used to create the initial 180DW, and subsequent 180DWs of opposing chirality were injected by applying fields of $|H_y| = 14.2 \text{ kA/m}$ in alternating directions. A SEMPA image of a stable 540DW is shown in Fig. 4(a). In this case, the applied field values were $+134 \text{ kA/m}$, -14.2 kA/m , $+14.2 \text{ kA/m}$, and -14.2 kA/m (this field sequence could have feasibly nucleated a 720DW). MFM imaging of the same sample cycled in a similar manner showed only a 180DW, suggesting that the field from the MFM tip destabilized the 540DW and led to a collapse into a simpler structure.

Fig. 4(b) is a SEMPA image of the sample of Fig. 4(a) after injection of a fourth 180DW. The additional wall is of the correct chirality to form a 720DW, but it was pinned before reaching the 540DW. The sample was then reset at $H_x = -80 \text{ kA/m}$ and cycled to introduce three 180DWs, which formed another 540DW of opposite rotation sense to the first one, shown in Fig. 4(c). The additional 180DW on the right of Fig. 4(c) is believed to be the remains of the original 540DW, which was not completely eliminated at -80 kA/m . Simulations of a 540DW show that it can persist until at least $H_x = 160 \text{ kA/m}$. These results demonstrate the possibility of creating DWs of $n\pi$ rotation ($n = \text{integer}$) in Co nanowires.

In summary, a method is presented for forming a 360° domain wall and more complex structures such as a 540° wall in a wire attached to an injection pad by applying an

alternating in-plane field perpendicular to the wire. SEMPA and OOMMF simulations give a consistent picture of the magnetic structure of the 360DW. The stray field distribution of a 360DW was modeled, and the expected MFM contrast was observed. In this way, MFM may be used to verify 360DWs. Equilibrium 360DWs in wires have a well-defined structure and size, persist over a wide field range, and can be distinguished from configurations consisting of two 180DWs pinned near each other. The formation and stability of these complex walls has implications in memory and logic devices based on field- or current-induced DW motion, where impingement of adjacent 180DWs can produce composite DWs whose behavior and stray field distribution differ significantly from that of a 180DW. These structures could also be used to examine intriguing resonant behavior as predicted by modeling.^{19,25}

Support of the National Science Foundation and the Nanoelectronics Research Initiative INDEX Center is gratefully acknowledged.

- ¹L. J. Heyderman, H. Niedoba, H. O. Gupta, and I. B. Puchalska, *J. Magn. Mater.* **96**, 125 (1991).
²H. W. Fuller, H. Rubinstein, and D. L. Sullivan, *J. Appl. Phys.* **32**, 286S (1961).
³D. O. Smith and K. J. Harte, *J. Appl. Phys.* **33**, 1399 (1961).
⁴J. Dean, A. Kohn, A. Kovacs, A. Zeltser, M. J. Carey, G. Hrkac, D. A. Allwood, and T. Schrefl, *J. Appl. Phys.* **110**, 073901 (2011).
⁵A. Hubert and R. Schäfer, *Magnetic Domains: The Analysis of Magnetic Microstructures* (Springer, Berlin, 1998).
⁶C. B. Muratov and V. V. Osipov, *J. Appl. Phys.* **104**, 053908 (2008).

- ⁷A. Kubetzka, O. Pietzsch, M. Bode, and R. Wiesendanger, *Phys. Rev. B* **67**, 020401R (2003).
⁸A. Kunz, *Appl. Phys. Lett.* **94**, 132502 (2009).
⁹M. D. Mascaró, C. Nam, and C. A. Ross, *Appl. Phys. Lett.* **96**, 162501 (2010).
¹⁰M. Laufenberg, D. Backes, W. Bühner, D. Bedau, M. Kläui, U. Rüdiger, C. A. F. Vaz, J. A. C. Bland, L. J. Heyderman, F. Nolting *et al.*, *Appl. Phys. Lett.* **88**, 052507 (2006).
¹¹M. Kläui, *J. Phys.: Condens. Matter* **20**, 313001 (2008).
¹²Y. Togawa, T. Kimura, K. Harada, T. Akashi, T. Matsuda, A. Tonomura, and Y. Otani, *Jpn. J. Appl. Phys.* **45**, L1322 (2006).
¹³M. T. Moneck and J. G. Zhu, *J. Appl. Phys.* **99**, 08H709 (2006).
¹⁴D. A. Allwood, G. Xiong, C. C. Faulkner, D. Atkinson, D. Petit, and R. P. Cowburn, *Science* **309**, 1688 (2005).
¹⁵S. S. P. Parkin, M. Hayashi, and L. Thomas, *Science* **320**, 190 (2008).
¹⁶M. Diegel, R. Mattheis, and E. Halder, *IEEE Trans. Magn.* **40**, 2655 (2004).
¹⁷F. J. Castaño, C. A. Ross, A. Eilez, W. Jung, and C. Frandsen, *Phys. Rev. B* **69**, 144421 (2004).
¹⁸M. Diegel, S. Glathe, R. Mattheis, M. Scherzinger, and E. Halder, *IEEE Trans. Magn.*, **45**, 3792 (2009).
¹⁹M. D. Mascaró and C. A. Ross, *Phys. Rev. B* **82**, 214411 (2010).
²⁰M. R. Scheinfein, J. Unguris, M. H. Kelley, D. T. Pierce, and R. J. Celotta, *Rev. Sci. Instrum.* **61**, 2501 (1990).
²¹J. Unguris, in *Magnetic Imaging and Its Applications to Materials*, edited by M. De Graef and Y. Zhu (Academic Press, Burlington, 2000), Vol. 36, pp. 167-303.
²²M. Donahue and D. Porter, OOMMF User's Guide, Version 1.0 (National Institute of Standards and Technology, Gaithersburg, MD, September 1999).
²³R. D. McMichael and M. J. Donahue, *IEEE Trans. Magn.* **33**, 4167 (1997).
²⁴F. J. Castaño, C. A. Ross, C. Frandsen, A. Eilez, D. Gil, H. I. Smith, M. Redjail, and F. B. Humphrey, *Phys. Rev. B* **67**, 184425 (2003).
²⁵P. E. Roy, T. Trypiniotis, and C. H. W. Barnes, *Phys. Rev. B* **82**, 134411 (2010).